Letter

Entanglement steering in adaptive circuits with feedback

Vikram Ravindranath [1], Yiqiu Han,[1] Zhi-Cheng Yang [2,3,*] and Xiao Chen[1]

[1]*Department of Physics, Boston College, Chestnut Hill, Massachusetts 02467, USA*
[2]*School of Physics, Peking University, Beijing 100871, China*
[3]*Center for High Energy Physics, Peking University, Beijing 100871, China*

The intensely studied measurement-induced entanglement phase transition has become a hallmark of nonunitary quantum many-body dynamics. Usually, such a transition only appears at the level of each individual quantum trajectory, and is absent for the density matrix averaged over measurement outcomes. In this work, we introduce a class of adaptive random circuit models with feedback that exhibit transitions in both settings. After each measurement, a unitary operation is either applied or not depending on the measurement outcome, which steers the averaged density matrix towards a unique state above a certain measurement threshold. Interestingly, the transition for the density matrix and the entanglement transition in the individual quantum trajectory in general happen at *different* critical measurement rates. We demonstrate that the former transition belongs to the parity-conserving universality class by explicitly mapping to a classical branching-annihilating random-walk process.

Introduction. Monitoring a quantum system can yield fascinating physics. The interplay between unitary dynamics and measurement creates an intriguing nonequilibrium phenomenon referred to as measurement-induced entanglement phase transitions (MIPTs) [1–6]. In its most commonly explored setting, an initial unentangled state is evolved by a random quantum circuit subject to measurements at a rate p. Above (below) a critical rate p_c, the steady state exhibits area-law (volume-law) entanglement scaling. To observe this transition, it is necessary to keep track of each individual quantum trajectory as the intrinsic randomness of measurement outcomes leads to the ensemble-averaged postmeasurement state being a maximally mixed density matrix ($\rho \propto \mathbb{1}$) in the allowed Hilbert space. As a result, the MIPT remains invisible to the ensemble-averaged density matrix, presenting significant challenges for experimental observation, with only a few exceptions [7–9].

Despite these challenges, midcircuit repeated measurements have become a valuable tool to create novel quantum phases dynamically. Recently, a new class of nonunitary dynamics has been proposed, where the outcome of a measurement can impact the dynamics themselves, leading to a nontrivial density matrix and stabilizing various quantum ordered phases through a feedback mechanism [10–15].

In this Letter, we introduce a class of adaptive random circuits with feedback that exhibits phase transitions for both the quantum trajectory and the ensemble-averaged density matrix (i.e., quantum channel), as depicted schematically in Fig. 1. In addition to varying the measurement rate p, the post-measurement state is also locally corrected conditioned on the measurement outcome with a feedback rate $0 \leqslant r \leqslant 1$. The

feedback is designed to "steer" the system towards particular final states. When $p \times r$ is large enough, the steady state is a mixture of two ferromagnetically ordered states instead of a maximally mixed state involving exponentially many configurations. Thus, there is an order-disorder phase transition in the quantum dynamics, which can be observed at the level of both quantum trajectory and quantum channel [12,13]. A similar order-disorder transition has also been discussed recently in the context of dissipative phase transitions [16,17]. However, we emphasize that the transitions discovered therein only exist in d dimension with $d \geqslant 2$ or 1D systems with long-range interactions. Instead, by explicitly mapping the motion of domain walls to a classical branching-annihilating random walk (BAW) process, we show that the order-disorder phase transition in our adaptive circuit model belongs to the parity-conserving (PC) universality class which exists in 1D [18–21]. Furthermore, the familiar MIPT is observed at the level of the quantum trajectory. Interestingly, we find that these two transitions typically occur at *different* critical measurement rates. Moreover, we show that the order-disorder phase transition can be probed experimentally from the measurement outcomes along the circuit evolution, and does not require post-selection.

Model. Our circuit model consists of three-qubit unitary gates and two-qubit measurements, as illustrated in Fig. 2. We take each three-qubit unitary gate to have a block structure: It leaves the basis states $|000\rangle$ and $|111\rangle$ unchanged up to a $U(1)$ phase (forming blocks of size one), and acts as a Haar random unitary within the six-dimensional subspace spanned by $\{|001\rangle, |010\rangle, |100\rangle, |011\rangle, |101\rangle, |110\rangle\}$. We measure the product of Pauli-Z operators across a bond between two consecutive sites $Z_i Z_{i+1}$. Crucially, our construction includes *feedback*: If an "undesired" measurement outcome $Z_i Z_{i+1} = -1$ is obtained (meaning that the post-measurement state is
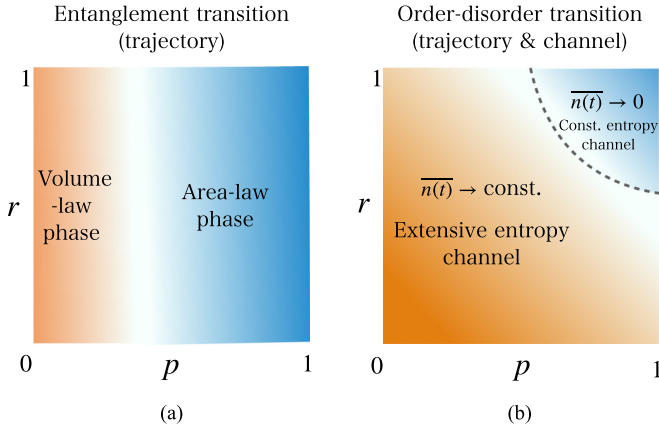
*zcyang19@pku.edu.cn

FIG. 1. Schematic phase diagram illustrating (a) the entanglement phase transition for the individual quantum trajectories and (b) domain wall density transition as a function of the measurement rate p and feedback rate r. The transition in (b) also signals an entropy transition *at the level of quantum channel* (ensemble-averaged density matrix). The critical line in (b) belongs to the PC universality class and satisfies $p \times r = \text{const}(\approx 0.55)$. The critical line in (a) is numerically upper bounded by $p_c^{EE} \leqslant 0.45$.

$|01\rangle$ or $|10\rangle$), we apply a Pauli-X operator on either site with probability r to correct the state into $|00\rangle$ or $|11\rangle$; if the measurement outcome is $+1$, then no operator is applied. A set of measurements and corrections is implemented in two layers—first over odd and then even bonds. In each layer, measurements are made at a rate p per bond. Each unit time step contains three layers of unitary gates related by a translation by one site, interspersed with a set of measurements after each of the first and second, but not third, layers. Time evolution for each unnormalized quantum trajectory is thus
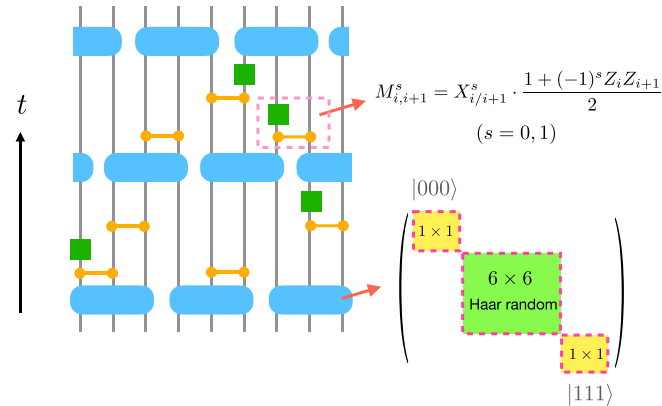

FIG. 2. Setup of the adaptive circuit with feedback (one time unit). The circuit consists of three-qubit unitary gates (denoted by blue boxes) and two-qubit measurements (orange lines with dotted end points). The unitary gate leaves $|000\rangle$ and $|111\rangle$ unchanged, and acts as a Haar random unitary within the complementary subspace. If the measurement outcome $Z_iZ_{i+1} = -1$, a Pauli-X operator (green box) is applied on one site to correct the post-measurement state into $|11\rangle$ or $|00\rangle$. Each unit time step contains three layers of unitary gates related by translation by one site, and two sets of measurements. Each set consists of an even and an odd layer, forming a brickwork structure.

given by

$$|\psi(\{s\}, T)\rangle = \prod_{t=1}^{T} [U_3(t)M_2(t)U_2(t)M_1(t)U_1(t)] |\psi_0\rangle$$
$$\equiv C(\{s\}) |\psi_0\rangle, \tag{1}$$

where U_j denotes the jth layer of unitary gates at each time step, $M_{1/2}$ denotes a set of measurements, and $\{s\}$ records the full set of measurement outcomes along this particular trajectory.

Akin to previous studies on measurement-induced phase transitions in hybrid random circuits, we expect that there is an MIPT in our setup for individual quantum trajectories [Fig. 1(a)]. Upon increasing the measurement rate p, there is a transition in the time-evolved states (1) from a volume-law entangled phase to a weakly entangled area-law phase, where the spins almost point along the $\hat{z}$ direction. Without feedback ($r = 0$), each spin could randomly point along $\pm\hat{z}$ directions in each trajectory, depending on the measurement outcomes. Upon introducing feedback, the final states in all trajectories will approach a ferromagnetically ordered state $\alpha|00\ldots0\rangle + \beta|11\ldots1\rangle$, provided that the measurement and feedback rates are large enough. This indicates that besides the MIPT, the steady state also exhibits an order-disorder transition in a physical observable—the domain wall density—due to feedback [Fig. 1(b)].[1] Since the expectation value of a physical observable is linear in the density matrix, the average domain-wall density evaluated for the trajectories and the quantum channel (trajectory-averaged density matrix)

$$\rho = \sum_{\{s\}} C(\{s\}) |\psi_0\rangle\langle\psi_0| C(\{s\})^{\dagger} \tag{2}$$

are equivalent. Hence, this order-disorder transition can be observed both in the individual trajectories and the quantum channel.

Phase transition in the domain-wall density. We demonstrate that there is indeed an order-disorder phase transition captured by the domain-wall density by mapping the dynamics of domain walls under the hybrid circuit evolution to a classical stochastic process. We write the time-evolved wave function as a sum of world histories: $|\psi(t)\rangle = \sum_{\{m(\tau)\}} A(\{m(\tau)\})|m\rangle$, where $\{|m\rangle\}$ are bit strings in the computational basis, and $A(\{m(\tau)\})$ is the amplitude of a particular world history $\{m(\tau)\}_{0\leqslant\tau\leqslant t}$. We consider each world history by constructing paths connecting bit-string configurations in the initial state to state at time t, as illustrated in Figs. 3(a) and 3(b).

Each individual path can be mapped to a classical stochastic process, which has a nonequilibrium phase transition. We denote the presence of each domain wall as a particle ●, and the absence of which as an empty site ○. The bit-string configuration is thus translated into one of particle occupations, as shown in Fig. 3(c). Under the action of unitary gates,

---

[1]In our model, the steady state persists until a timescale $t \sim \text{poly}(L)$ with a power $\geqslant 2$. For $t \sim \exp(L)$, the states will eventually approach a ferromagnetically ordered state, and both the entanglement and order-disorder phase transitions no longer exist.

(a)

(b)

Bit string: 101110001011

Domain wall: 1 ● 0 ● 111 ● 000 ● 1 ● 0 ● 11

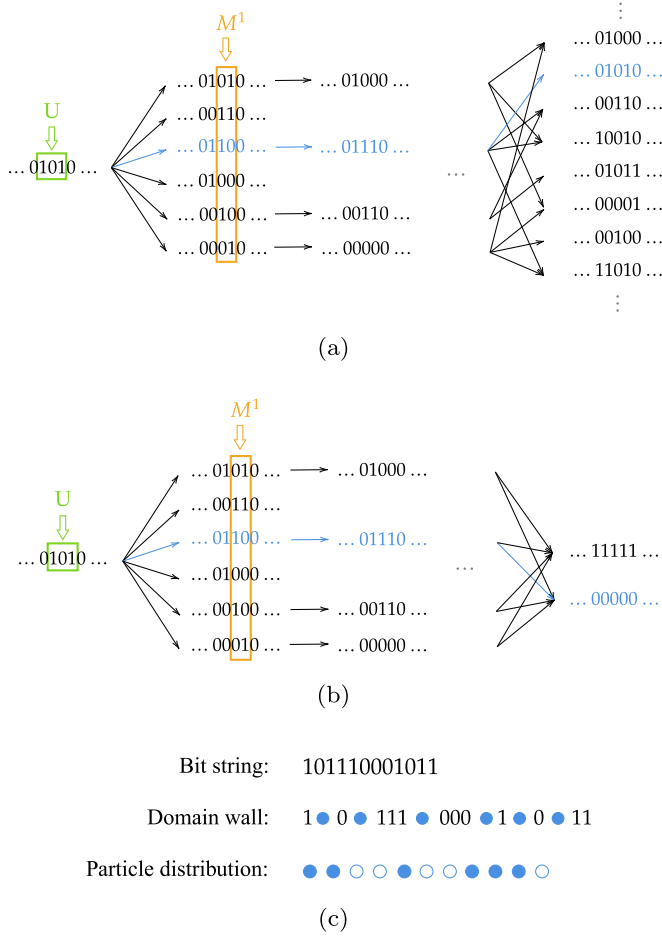Particle distribution: ● ● ○ ○ ○ ● ○ ○ ● ● ○

(c)

FIG. 3. (a),(b): Illustration of the bitstring dynamics in the quantum trajectory undergoing hybrid circuit evolution. The blue arrows indicate two representative paths ("world histories") of the bitstring dynamics. (a) When the measurement rate is small, the steady state involves exponentially many bistring configurations. (b) When the measurement rate is high, the steady state is spanned by two ordered bitstrings. (c) Mapping from a bitstring configuration to particle distribution, where a particle and an empty site represent the presence and absence of a domain wall, respectively.

the particles undergo two types of processes: ● ○ ○ ↔ ● ● ● (branching), and diffusion. Under measurement, the particles can either diffuse, ●○ ↔ ○●, or annihilate in pairs with probability $q \equiv pr$, ●● → ○○. Combining these processes together, the particles perform BAW with an even number of offspring:

$$W \leftrightarrow 3W, \quad W + W \overset{q}{\to} \emptyset. \tag{3}$$

Since the parity of the total particle number is conserved, the classical dynamics described above belongs to the PC universality class, which has a continuous dynamical phase transition when the rate of particle annihilation exceeds a certain threshold [18–21] [see Supplemental Material (SM) [22] for more details]. The two phases can be distinguished in terms of the average particle (domain wall) density in the steady state $n(t) = N(t)/L$.

For initial conditions with an extensive number of particles $N \propto L$, $n(t)$ saturates to a finite constant when $q < q_c$ after a finite amount of time. When $q > q_c$, $n(t) \sim t^{-1/2}$, and decays

to zero at $t \sim L^2$ if the initial state has an even number of particles. At q_c, $n(t) \sim t^{-\theta}$ with a universal exponent $\theta = 0.286$ characteristic of PC universality class. For the initial condition with two adjacent particles, when $q < q_c$, the particle density grows linearly in time and saturates to a finite constant. At $q = q_c$, the particle density remains constant. When $q > q_c$, the particle density decays as $t^{-1/2}$. Therefore, our model exhibits an order-disorder phase transition at a critical effective measurement rate q_c. Below, we shall explicitly demonstrate both transitions depicted in Fig. 1 via numerical simulations of the hybrid circuit dynamics.

Numerical results. In our simulations, initial states, which are product states in the computational basis, are evolved according to the setup in Fig. 2 with open boundary conditions. We record, at each time step, the second Rényi entropy $S_A^{(2)}(t) = -\log(\text{tr}\rho_A^2)$, where ρ_A denotes the reduced density matrix of subsystem A composed of sites $1, 2 \dots |A|$; $1 \leqslant |A| \leqslant \frac{L}{2}$, and the domain-wall density

$$n(t) \equiv \frac{1}{L-1} \sum_{i=1}^{L-1} \left\langle \frac{1 - Z_i Z_{i+1}}{2} \right\rangle_t. \tag{4}$$

We then compute the trajectory-averaged second Rényi entropy $\overline{S_A^{(2)}(t)}$ and domain-wall density $\overline{n(t)}$. It is worth noting that in experimental platforms, the determination of $\bar{n}$ does not require an extra step; the measurement outcomes for any $p > 0$ provide an accurate sampling of $n(t)$. Our simulations are performed using the ITENSOR JULIA package [23,24] based on a matrix product state representation of the time-evolved wave functions.

We first set $p = 1$, and study $\overline{n(t)}$ as r is varied (along the right boundary of Fig. 1). Since the system is expected to be in the area-law phase, this serves as a benchmark to observe the order-disorder phase transition as revealed by the domain-wall density $\overline{n(t)}$. Starting from a random state with $n(t = 0) \approx \frac{1}{2}$, we find clear evidence that the steady state is area-law entangled and is independent of r (data not shown). Further study of $\overline{n(t)}$ indicates that when $r \lesssim 0.2$, $\overline{n(t)}$ saturates to a finite constant at long times; on the other hand, when $r \gtrsim 0.8$, $\overline{n(t)} \sim t^{-1/2}$ as shown in Fig. 4. This indicates the existence of two phases within the area-law entangled phase, distinguished by $\overline{n(t)}$. However, owing to finite-size effects, $\overline{n(t)}$ appears to decay with a continuously varying exponent] i.e., $n(t) \sim t^{-\theta_{n_0=0.5}(r)}$] for $0.2 \lesssim r \lesssim 0.8$, which makes identifying the critical r_c difficult. Instead, we consider an initial state with two neighboring domain walls centered in the lattice. Again, $n(t) \sim t^{\theta_{N_0=2}(r)}$ with a continuously varying exponent in the intermediate regime, but the critical point r_c is determined by the rate r at which $\overline{n(t)} \sim$ const [or equivalently, when $\theta_{N_0=2}(r_c) \approx 0$ and changes sign]. Using this criterion, we find that $r_c \approx 0.55$ in Fig. 5(a).

Next, we study the dynamics upon varying p, while fixing $r = 1$ (along the top boundary of Fig. 1). In this case, we expect to observe an entanglement phase transition *and* a transition in $\overline{n(t)}$. In Fig. 5(b), we find an order-disorder transition as revealed by $\overline{n(t)}$ at $p_c^n \approx 0.55$. In fact, we find, by considering various values of p and r, that the order-disorder transition in our system is controlled by a single parameter $q \equiv pr$, and happens at $q_c \approx 0.55$ [see Fig. 5(c)], confirming our mapping
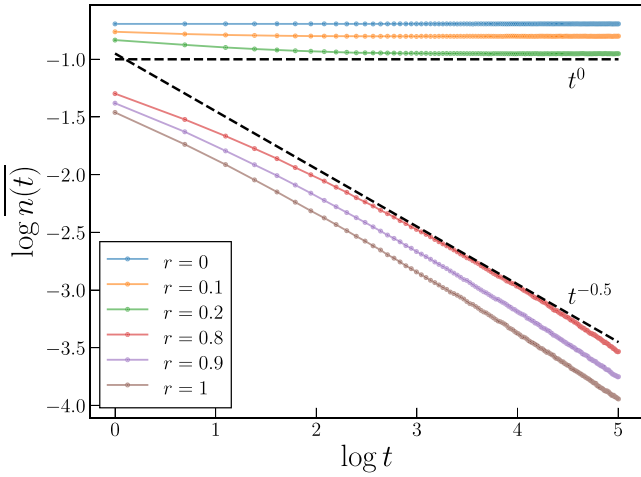
FIG. 4. The trajectory-averaged domain-wall density $\overline{n(t)}$ as a function of time, for different values of the feedback rate r while fixing $p = 1$, starting from random initial states. The result confirms the existence of two phases. Numerical simulations are performed for $L = 300$, and averaged over 10^4 realizations of circuits and initial states.

to a classical BAW process in Fig. 3. An interesting question that naturally arises is whether the location of the order-disorder transition in $\overline{n(t)}$ coincides with that of the MIPT.

The computational resources required to simulate the system increase exponentially as one nears the critical point p_c^{EE} of the MIPT from above. Nonetheless, we provide strong evidence that these two transitions happen at *different* points in our system. As we further lower p such that $p < p_c^n \approx 0.55$, we find that the system remains in the area-law entangled phase despite a finite domain-wall density, as is demonstrated by the scaling of $\overline{S_A^{(2)}}$ with subsystem size in Fig. 6(a). In the SM, we provide a heuristic argument based on the correlation length to explain why these two transitions in general should be different. We thus conclude that the critical point for the
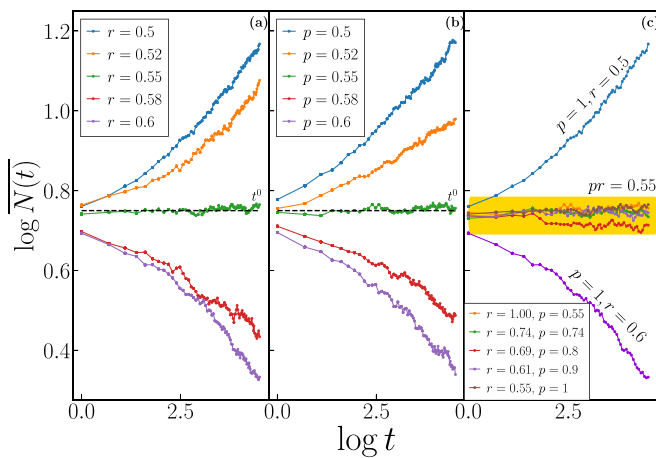

FIG. 5. The averaged number of domain walls $\overline{N(t)}$ starting from an initial state with two domain walls. (a) For $p = 1$, the exponent θ as in $\overline{n(t)} \sim t^\theta$ changes sign at $r_c \approx 0.55$. (b) For $r = 1$, $p_c^n \approx 0.55$. (c) Demonstration that the order-disorder transition in $\overline{n(t)}$ is governed by a single parameter $q \equiv pr$.
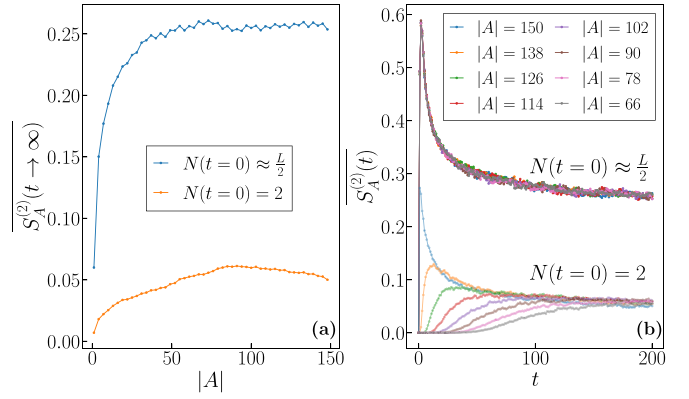

FIG. 6. (a) The steady-state entanglement entropy remains independent of subsystem size, regardless of the initial state. (b) The difference in the early time growth visualized across different initial conditions and subsystem sizes. In both figures, $p = 0.45 < p_c^n$ and $r = 1$.

MIPT $p_c^{EE} < p_c^n$. This is also consistent with the general expectation that the entanglement transition for the individual trajectories must precede that for the quantum channel, if there is one.

Discussion. The physics discussed in this work remains unchanged if the three-qubit unitary gates are replaced by k-qubit unitary gates ($k > 3$) which leave $\underbrace{|00\ldots0\rangle}_{k}$ and $\underbrace{|11\ldots1\rangle}_{k}$ invariant [up to a $U(1)$ phase] and act as Haar random unitaries within the remaining $(2^k - 2)$-dimensional subspace. When $k = 2$, however, the local unitary gates coincide with those for a $U(1)$-symmetric Haar random circuit. As a result, the particles can only spread out diffusively rather than ballistically and hence cannot compete with any nonzero rate of particle annihilations induced by feedback. $\overline{n(t)}$ always decays as $t^{-1/2}$ for any $q > 0$; there is *no* MIPT and individual trajectories are immediately driven to an area-law entangled phase [22]. This is in sharp contrast to $U(1)$-symmetric hybrid circuits without feedback, where an MIPT is present [25].

In this work, we have argued that the two transitions—MIPTs and order-disorder transitions—are generally unrelated. As we increase r, the difference between p_c^{EE} and p_c^n becomes smaller but remains finite when $r = 1$. In the SM, we consider models in which the essential physics is unchanged, but the difference between these two transitions is more pronounced. This is in contrast to a free fermion system subject to nonunitary dynamics with feedback that was recently studied in Ref. [13]. It remains to be seen if models with interactions can exhibit these transitions at the same point, while a broader understanding of the conditions that can facilitate this coincidence of these transitions is desirable.

We conclude by commenting on the experimental realizability of the order-disorder transition, spurred by the recent implementation of adaptive quantum circuits with high fidelity [14,15]. Overhead can be drastically reduced by estimating $\overline{n(t)}$ from measurement outcomes obtained over the course of the circuit evolution, instead of preparing the states at different times and then separately performing measurements. Furthermore, we numerically find that this transition is

[1] Y. Li, X. Chen, and M. P. A. Fisher, Quantum zeno effect and the many-body entanglement transition, Phys. Rev. B **98**, 205136 (2018).

[2] Y. Li, X. Chen, and M. P. A. Fisher, Measurement-driven entanglement transition in hybrid quantum circuits, Phys. Rev. B **100**, 134306 (2019).

[3] B. Skinner, J. Ruhman, and A. Nahum, Measurement-Induced Phase Transitions in the Dynamics of Entanglement, Phys. Rev. X **9**, 031009 (2019).

[4] A. Chan, R. M. Nandkishore, M. Pretko, and G. Smith, Unitary-projective entanglement dynamics, Phys. Rev. B **99**, 224307 (2019).

[5] M. J. Gullans and D. A. Huse, Dynamical Purification Phase Transition Induced by Quantum Measurements, Phys. Rev. X **10**, 041020 (2020).

[6] S. Choi, Y. Bao, X.-L. Qi, and E. Altman, Quantum Error Correction in Scrambling Dynamics and Measurement-Induced Phase Transition, Phys. Rev. Lett. **125**, 030505 (2020).

[7] M. Ippoliti and V. Khemani, Postselection-Free Entanglement Dynamics via Spacetime Duality, Phys. Rev. Lett. **126**, 060501 (2021).

[8] C. Noel, P. Niroula, D. Zhu, A. Risinger, L. Egan, D. Biswas, M. Cetina, A. V. Gorshkov, M. J. Gullans, D. A. Huse *et al.*, Measurement-induced quantum phases realized in a trapped-ion quantum computer, Nat. Phys. **18**, 760 (2022).

[9] J. M. Koh, S.-N. Sun, M. Motta, and A. J. Minnich, Measurement-induced entanglement phase transition on a superconducting quantum processor with mid-circuit readout, Nat. Phys. (2023).

[10] M. McGinley, S. Roy, and S. A. Parameswaran, Absolutely Stable Spatiotemporal Order in Noisy Quantum Systems, Phys. Rev. Lett. **129**, 090404 (2022).

[11] A. J. Friedman, O. Hart, and R. Nandkishore, Measurement-induced phases of matter require adaptive dynamics, arXiv:2210.07256.

[12] T. Iadecola, S. Ganeshan, J. Pixley, and J. H. Wilson, Dynamical entanglement transition in the probabilistic control of chaos, arXiv:2207.12415.

[13] M. Buchhold, T. Mueller, and S. Diehl, Revealing measurement-induced phase transitions by pre-selection, arXiv:2208.10506.

[14] M. Iqbal, N. Tantivasadakarn, T. M. Gatterman, J. A. Gerber, K. Gilmore, D. Gresh, A. Hankin, N. Hewitt, C. V. Horst, M.

[15] Matheny *et al.*, Topological order from measurements and feed-forward on a trapped ion quantum computer, arXiv:2302.01917.

[15] M. Foss-Feig, A. Tikku, T.-C. Lu, K. Mayer, M. Iqbal, T. M. Gatterman, J. A. Gerber, K. Gilmore, D. Gresh, A. Hankin *et al.*, Experimental demonstration of the advantage of adaptive quantum circuits, arXiv:2302.03029.

[16] P. Sierant, G. Chiriacò, F. M. Surace, S. Sharma, X. Turkeshi, M. Dalmonte, R. Fazio, and G. Pagano, Dissipative Floquet dynamics: From steady state to measurement induced criticality in trapped-ion chains, Quantum **6**, 638 (2022).

[17] N. Lang and H. P. Büchler, Exploring quantum phases by driven dissipation, Phys. Rev. A **92**, 012128 (2015).

[18] M. Henkel, H. Hinrichsen, S. Lübeck, and M. Pleimling, *Non-Equilibrium Phase Transitions* (Springer, New York, 2008), Vol. 1.

[19] D. Zhong and D. ben Avraham, Universality class of two-offspring branching annihilating random walks, Phys. Lett. A **209**, 333 (1995).

[20] K. Park, H. Hinrichsen, and I.-m. Kim, Binary spreading process with parity conservation, Phys. Rev. E **63**, 065103(R) (2001).

[21] Y. Han and X. Chen, Measurement-induced criticality in z_2-symmetric quantum automaton circuits, Phys. Rev. B **105**, 064306 (2022).

[22] See Supplemental Material at http://link.aps.org/supplemental/10.1103/PhysRevB.108.L041103 for additional numerical results and discussions on particle density transition of the classical bit-string dynamics, models with one set of measurements, effects of imperfect circuits, sampling protocol for estimating the domain-wall density experimentally, a heuristic argument for the separation of the entanglement and absorbing state transitions, and simulation of the volume-law phase.

[23] M. Fishman, S. R. White, and E. M. Stoudenmire, The ITensor Software Library for Tensor Network Calculations, SciPost Phys. Codebases, 4 (2022).

[24] M. Fishman, S. R. White, and E. M. Stoudenmire, Codebase release 0.3 for ITensor, SciPost Phys. Codebases, 4-r0.3 (2022).

[25] U. Agrawal, A. Zabalo, K. Chen, J. H. Wilson, A. C. Potter, J. H. Pixley, S. Gopalakrishnan, and R. Vasseur, Entanglement and Charge-Sharpening Transitions in U(1) Symmetric Monitored Quantum Circuits, Phys. Rev. X **12**, 041002 (2022).

[26] N. O'Dea, A. Morningstar, S. Gopalakrishnan, and V. Khemani, Entanglement and absorbing-state transitions in interactive quantum dynamics, arXiv:2211.12526.